Check for updates

Effect of Er doping on the In$_2$O$_3$(001) surface for H$_2$S, NO$_2$, and CO detection: a DFT study

Neha Sharma[ab] and Sandip Paul Choudhury [ID] *[a]

The impact of Erbium (Er) doping on the gas sensing performance of the In$_2$O$_3$(001) surface toward H$_2$S, NO$_2$, and CO was rigorously investigated using density functional theory (DFT) calculations. Analysis based on adsorption energy, Bader charge transfer, and density of states (DOS) confirms that Er doping selectively enhances the surface reactivity toward NO$_2$. Key results demonstrate a marked improvement in NO$_2$ binding strength: the adsorption energy increases significantly from −0.37 eV on the pristine surface to −0.61 eV on the Er-doped surface. This stronger chemisorption is supported by enhanced electron withdrawal from the surface by NO$_2$, with the charge transfer increasing from −0.38 e (pristine) to −0.46 e (Er-doped). Furthermore, TDOS and PDOS analyses confirm the appearance of new, strong electronic states near the Fermi level only after NO$_2$ adsorption on the doped surface, indicating robust electron coupling. Conversely, Er doping weakens the interaction with the other test gases. For H$_2$S, the adsorption energy reduces from −0.53 eV to −0.42 eV, and charge transfer drops sharply from +0.40 e to +0.09 e. CO adsorption remains weak, with the energy decreasing slightly from −0.25 eV to −0.19 eV. These findings indicate that Er-doped In$_2$O$_3$(001) surfaces exhibit enhanced selectivity, making them highly promising candidates for selective NO$_2$ detection.

1. Introduction

The increment of industrial production has led to environmental problems, one of which is air pollution, which cannot be avoided. The source of air pollution is gaseous pollutants that are released by vehicles and industries. These can have adverse effect on human health and the environment.[1] The solution to this problem is precisely identifying the harmful gas pollutants present in the industrial exhaust. Gas sensors are often the usual method to detect these gases.[2] Metal oxide semiconductor-based gas sensors are often used to detect gases because of many features including low cost, high sensitivity, high stability, and ease of fabrication.[3]

Metal oxide semiconductors (MOSs) such as ZnO, WO$_3$, SnO$_2$ and In$_2$O$_3$ are used as a gas sensing material in many gas sensors because of their easy fabrication process, low cost and good performance.[4] Among these, indium oxide (In$_2$O$_3$) is a promising sensing material due to its high conductivity, adjustable shape and size, good catalytic properties and abundant defects. In$_2$O$_3$ is an n-type metal oxide semiconductor (MOS) with a wide band gap of 3.75 eV (direct) and 2.61 eV (indirect).[5] Studies on various morphologies, such as nanoparticles, nanofibers, nanosheets

and nanoflowers, have been conducted for environmental pollutant gases (NO$_2$, CO and H$_2$S) to increase sensitivity and selectivity.[6] Some progress has been made for pristine In$_2$O$_3$-based gas sensors to overcome the selectivity and operating temperature issue.[7] Doping is an efficient way to overcome these issues because a small amount of dopant may convert the nonporous structure to a porous structure and provide defect states, which is good for gas sensing.[8,9]

Nowadays, rare earth elements (REEs) are emerging to solve these problems because they have 4f orbitals with partially filled electrons. When a rare earth element (RE^{3+}) is added to indium oxide (In$_2$O$_3$), it can easily take the place of In^{+3} because of the similarity in their ionic radii. This replacement causes some strain in the crystal structure of In$_2$O$_3$.[10] Among them, europium (Eu) and erbium (Er) are particularly interesting for In$_2$O$_3$ due to their stable trivalent oxidation state (Eu^{3+}/Er^{3+}), which allows substitution at indium sites with minimal lattice distortion. Eu-doping has been shown to enhance charge transfer and adsorption capability, improving the surface reactivity of In$_2$O$_3$ toward gas molecules. On the other hand, Er possesses a slightly smaller ionic radius and a distinct 4f electronic configuration, which can further modify the band structure and facilitate stronger interactions with adsorbed species. A study by Zhou *et al.*[11] reported that hydrothermally synthesized 3 wt% Ce-doped In$_2$O$_3$ as compared to the pristine In$_2$O$_3$ has a better response for *n*-butanol gas. They observed that 3 wt% Ce-doped In$_2$O$_3$ has a response

[a] Department of Physics, Amity School of Applied Science, Amity University Rajasthan, Jaipur, Rajasthan – 303002, India.
E-mail: sandip.pchoudhury@gmail.com
[b] Department of Physics, JECRC Foundation, Jaipur, Rajasthan – 302022, India

value of 225.3 for 100 ppm *n*-butanol gas at an optimum temperature of 320 °C, which was 3.7 times higher than that of pure In_2O_3. Wang *et al.*[12] synthesized In_2O_3 and Er-doped In_2O_3 nanotubes by an electrospinning method followed by calcination. They observed that the synthesized Er-doped In_2O_3 has 4 times the response value than that of pure In_2O_3 for 20 ppm formaldehyde (HCHO) gas at 260 °C temperature. Qin *et al.* reported that the carbon thermal reduction method was utilized for the synthesis of pure and Er-doped In_2O_3 nanoribbons.[13] The Er doping in In_2O_3 reduces the optimal temperature from 260 °C to 220 °C and also increases the sensitivity of 100 ppm ethanol from 2.4 to 4.8. It shows better selectivity towards interfering gases such as CO, H_2S, HCHO and NO_2. They observed that Er doping reduced the operating temperature for alcohol detection, and a fast response and recovery time were achieved for different alcohol concentrations at 220 °C. Liu *et al.* performed a DFT study to evaluate the adsorption effect of gases such as H_2, CO and CH_4 on the $In_2O_3(110)$ surface. The calculation results based on DFT indicate that intrinsic In_2O_3 is not optimum for H_2, CO and CH_4 adsorption, while Ag-decorated In_2O_3 shows optimum sensing for these gases.[3] Chen *et al.*[14] reported that the Eu-doped In_2O_3 nanobelts exhibit higher sensitivity towards H_2S gas as compared to pure In_2O_3. They showed that Eu doping enhances the sensitivity of H_2S gas by five times compared to undoped In_2O_3. Eu-doped In_2O_3 exhibits better selectivity towards to H_2S gas with interfering gases such as CO, NO_2, HCHO and ethanol at 260 °C temperature.

The novelty of the present study lies in providing a comparative mechanistic understanding of gas adsorption on rare earth element (REE)-doped In_2O_3 surfaces. The present study explores Er and Eu-doped In_2O_3 systems for gas-sensing applications at the DFT level, which have not been previously explored. Earlier DFT studies on In_2O_3 mainly focused on pristine and transition metal-doped surfaces and their analysis was limited to single gas adsorption. In contrast, our DFT investigation systematically examines the adsorption behaviour of multiple gases (H_2S, NO_2, and CO), analysing adsorption energies, charge density differences (CDD), and density of states (DOS). All calculations were performed using Quantum Espresso on a hexagonal In_2O_3 unit cell (space group $R\bar{3}c$). Compared with previous theoretical investigations on In_2O_3 surfaces, the present DFT study provides several distinctive contributions. First, the (001) surface of In_2O_3 was chosen, which is less explored but exhibits high surface reactivity relevant for gas sensing applications. Second, the study systematically examines the influence on the electronic structure and gas adsorption properties of rare-earth element Er. Third, a comparative analysis of H_2S, NO_2, and CO adsorption is performed to elucidate NO_2 selectivity based on adsorption energy, charge density difference, and DOS evolution. This approach provides atomistic insight into how the Er dopant modulates surface reactivity and charge transfer characteristics, thereby guiding towards a more reliable rare-earth-element-doped In_2O_3 gas sensor.

2. Computational details

2.1. Software and parameters

Quantum Espresso (QE) software, based on density functional theory (DFT), was employed for the computational work. The Perdew–Burke–Ernzerhoff (PBE) functional was used in these calculations to treat the exchange–correlation inside the general gradient approximation (GGA), while ultrasoft pseudopotentials were used to characterise the electron–ion interactions.[15] In the current work, the energy cut-offs of 50 and 450 Ryd for the wave functions and charge densities were used to calculate the band structure and other parameters. All calculations were performed using a $2 \times 2 \times 2$ k-point mesh, except DOS, which, after optimisation, employed a dense k-point grid ($6 \times 6 \times 2$). Similar k-point sampling ($2 \times 2 \times 1$) was successfully used for 60-atom $In_2O_3(110)$ surface models employing DFT-D2 methods, demonstrating the reliability of the present setup.[3] To determine the surface reliability, different In_2O_3 surfaces were employed but the $In_2O_3(001)$ surface gave the best results. For each structure, a vacuum layer of 15 Å was created along the z-direction to remove interference from nearby layers.

2.2. Surface model

We chose the In_2O_3 hexagonal crystal system for this work. This hexagonal unit cell of In_2O_3 is made up of 12 In and 18 O atoms, with lattice parameters of $a = b = 5.5162$ Å and $c = 14.5911$ Å, which is equivalent to the experimental value.[16] The $In_2O_3(001)$ surface was selected for this study. It is represented by a $2 \times 2 \times 1$ In_2O_3 supercell, which is cleaved by the plane 001 which contains 120 atoms. Furthermore, the cell width was reduced from 1 to 0.5 to obtain the $In_2O_3(001)$ two-layer surface with a total of 60 atoms. For the defect In_2O_3 surfaces one was replaced by one rare earth element Er. All structures were optimized without and with the adsorbate gas molecules (CO, NO_2, and H_2S) as shown in Fig. 1. The relaxed structure represents that the Er-doping creates a more compact structure. After NO_2 gas molecule adsorption, the compact behaviour is reduced.

The adsorption energy was calculated by the quantitative analysis of gas molecule interaction with the $In_2O_3(001)$ surface by the following equation[17,18]

$$\Delta E_{adsorption} = E_{surface+gas\ molecule} - E_{surface} - E_{gas\ molecule}$$

(1)

where, $\Delta E_{adsorption}$, $E_{surface+gas\ molecule}$, $E_{surface}$ and $E_{gas\ molecule}$ represent the adsorption energy, total energy of the surface with a gas molecule, total energy of the surface, and total energy of the gas molecule, respectively. The adsorption energy of defect/doped surfaces was calculated by eqn (2)

$$\Delta E_{adsorption} = E_{defect\ surface+gas\ molecule} - E_{defect\ surface}$$
$$- E_{gas\ molecule}$$

(2)

where $\Delta E_{adsorption}$, $E_{defect\ surface+gas\ molecule}$, $E_{defect\ surface}$ and $E_{gas\ molecule}$ represent the adsorption energy, total energy of the defect/doped surface with a gas molecule, total energy of

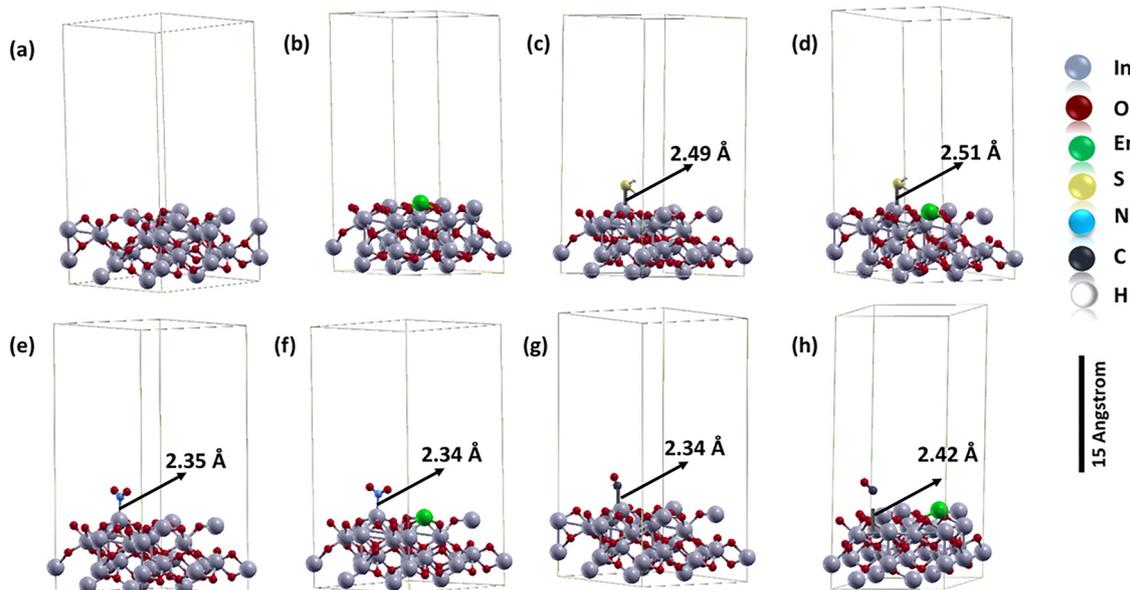This journal is © the Owner Societies 2025

Phys. Chem. Chem. Phys., 2025, **27**, 25440–25448 | **25441**

Fig. 1 Optimized geometries of (a) the pure In$_2$O$_3$(001) surface, (b) Er-doped In$_2$O$_3$(001) surface, and adsorption of H$_2$S, NO$_2$, and CO molecules on the top In atom site of (c), (e) and (g) pure and (d), (f) and (h) Er-doped In$_2$O$_3$(001) surfaces, respectively. The arrows indicate the adsorption distances between the surface atoms and the gas molecules. The 15 Å scale bar represents the vacuum region introduced along the z-direction to prevent interlayer interactions.

the defect surface, and total energy of the gas molecule, respectively.

3. Results and discussion

3.1. Adsorption energy analysis

The strength of the adsorbate's binding to the substrate (pure and Er-doped In$_2$O$_3$(001)) is commonly indicated by adsorption energy. The total energy of the adsorption system will be less than the sum of the energies of the substrate and the adsorbate if the adsorption is thermodynamically favourable, leading to a negative adsorption value. The physisorption and chemisorption processes can be identified by the magnitude of the adsorption energies.[19]

The adsorption energies of H$_2$S, NO$_2$ and CO were calculated on both pristine and Er-doped In$_2$O$_3$ surfaces using eqn (1) and (2). The adsorption energies were calculated for different Er-doped sites in In$_2$O$_3$. Among them, the configuration in which the first Er atom replaced the first indium (In) atom on the In$_2$O$_3$(001) upper surface was found to be the most favourable. The adsorption energy for NO$_2$, Er-doping significantly enhanced the adsorption strength (from −0.379 eV to −0.61 eV) (as shown in Table 1), indicating improved sensing potential. However, for H$_2$S and CO, the adsorption strength slightly decreased upon Er incorporation. The decrease in H$_2$S adsorption energy (−0.53 eV to −0.42 eV) remains within an acceptable sensing range, suggesting moderate sensing capability. CO adsorption energies remained weak in both cases (−0.25 eV to −0.19 eV), indicating poor interaction with surfaces. These findings suggest that Er-doping on the In$_2$O$_3$ surface increases the adsorption of the NO$_2$ molecule while

Table 1 Adsorption energies and charge transfer values through Bader charge analysis for pure and Er-doped In$_2$O$_3$(001) surfaces

S. no.	Gases	Adsorption energy (eV)		Charge transfer values	
		Pure In$_2$O$_3$(001) surface	Er-doped In$_2$O$_3$(001) surface	Pure In$_2$O$_3$(001) surface	Er-doped In$_2$O$_3$(001) surface
1.	NO$_2$	−0.37	−0.61	−0.3855e	−0.4596e
2.	H$_2$S	−0.53	−0.42	+0.4053e	+0.0927e
3.	CO	−0.25	−0.19	+0.0312e	+0.0711e

diminishing the adsorption of H$_2$S and CO molecules. This suggests that erbium (Er) doping selectively enhances the sensitivity of In$_2$O$_3$ toward NO$_2$.

3.2. Bader charge analysis

Bader charge analysis was employed to evaluate the effect of Er doping on the In$_2$O$_3$ surface. The pure and Er-doped In$_2$O$_3$ surfaces exhibit noticeable difference in Bader charge, attributed to the incorporation of the Er-dopant. While the lower surface layers show minimal variation, significant changes are observed in the upper surface atoms where the doping is introduced. These changes indicate that the Er dopant modifies the surface electronic structure and charge distribution of the In$_2$O$_3$ surface.

Also, Bader charge analysis was performed to evaluate the charge transfer between gas molecules and the surfaces (In$_2$O$_3$ and Er-doped In$_2$O$_3$). The charge transfer results indicate distinct gas adsorption behaviours for the pure and Er-doped In$_2$O$_3$ systems. The net charge transfer values for gas molecules

25442 | Phys. Chem. Chem. Phys., 2025, **27**, 25440–25448

This journal is © the Owner Societies 2025

on In_2O_3 and Er-doped In_2O_3 surfaces were examined through the following equation:

$$\Delta Q = Q_a - Q_b \qquad (3)$$

where, ΔQ, Q_a and Q_b represent the net charge transfer, charge on the gas molecule after adsorption and charge on the gas molecule before adsorption (isolated gas molecule).[20]

For H_2S, the pure In_2O_3 surface shows a significantly higher charge transfer (+0.4053 e) than the Er-doped surface (+0.0927 e), suggesting stronger adsorption on the undoped material. Conversely, for NO_2, the Er-doped In_2O_3 surface exhibits a more negative charge transfer (-0.4596 e) as compared to the pure In_2O_3 surface (-0.3855 e), implying enhanced electron donation, and thus stronger adsorption upon doping. The CO molecule, however, exhibits very low charge transfer performance for both the surfaces In_2O_3 and Er-doped In_2O_3 +0.0312 e, +0.0711 e, respectively. The CO molecule interaction reduces slightly on the Er–In_2O_3 surface. This indicates that a weak physisorption process occurs for the CO gas molecule. The charge transfer values are consistent with the results of adsorption energy. These findings reveal that Er-doping improves the NO_2 sensing selectivity, while a pure In_2O_3 surface is more favourable for H_2S gas detection.

3.3. Analysis of charge density difference (CDD) plot

In the CDD plot, the individual isolated system's charge densities are subtracted from the absorbed entire system's charge density. It reflects the charge redistribution caused by the interaction between gas molecules and the material's surfaces. The CDD provides information about charge accumulation and depletion around surfaces and gas molecules. The CDD plot is obtained by the given formula:[21,22]

$$\Delta\rho = \rho_{\text{surface+gas molecule}} - \rho_{\text{isolated surface}} - \rho_{\text{isolated gas molecule}} \qquad (4)$$

where $\Delta\rho$, $\rho_{\text{surface+gas molecule}}$, $\rho_{\text{isolated surface}}$ and $\rho_{\text{isolated gas molecule}}$ represent the charge density difference, charge density of the gas molecule adsorbed surface, charge density without a gas molecule, and charge density of an isolated gas molecule, respectively.

The CDD plots for the intrinsic $In_2O_3(001)$ surface and Er-doped $In_2O_3(001)$ surface upon adsorption of gases H_2S, NO_2 and CO are shown in Fig. 2. The CDD plot gives a qualitative analysis of Bader charge analysis. For H_2S gas, the CDD plot of In_2O_3 and Er-doped In_2O_3 shows a delocalized distribution of charges between the surface and gas molecule. In CDD plots, the yellow colour indicates the charge accumulation while cyan colour indicates the charge depletion.[23] The Bader charge transfer of +0.4053 e for H_2S on the In_2O_3 surface indicates that the gas molecules donate electrons from the surface. In the corresponding CDD plot, cyan lobes appear around the H_2S molecule, confirming charge depletion, while yellow lobes on the surface (at the lower surface around the In and O atoms) indicate charge accumulation (as shown in Fig. 2(a)). This indicates a sign of electron transfer from the gas molecule to the surface. Similar behaviour is observed for the Er-doped In_2O_3 surface, but charge transfer reduces to 0.09 e, which is reflected by light yellow and cyan colours. For NO_2 gas absorption, the CDD plot exhibits both yellow (accumulation) and cyan (depletion) lobes around the NO_2 molecule and the Er-doped In_2O_3 surface, indicating localized charge redistribution.[24] However, Bader charge analysis reveals a net negative charge transfer to the gas molecule, confirming that NO_2 withdraws electrons from the surface and acts as an electron acceptor.[25] For H_2S adsorption on pure and Er-doped In_2O_3 surfaces, the lobes are not localized at one atom, which reflects surface wide interaction
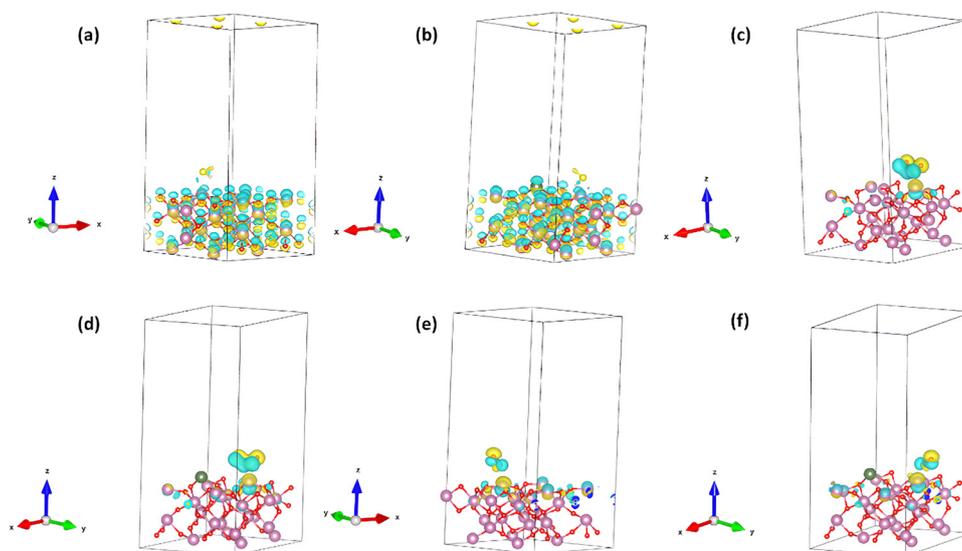
Fig. 2 CDD plots of (a), (c) and (e) pure and (b), (d) and (f) Er–doped $In_2O_3(001)$ surfaces after gas adsorption: (a) and (b) H_2S, (c) and (d) NO_2, and (e) and (f) CO. Pink, red, and dark green spheres represent indium (In), oxygen (O), and erbium (Er) atoms, respectively. Blue, brown, white, and black spheres denote nitrogen (N), sulphur (S), hydrogen (H), and carbon (C) atoms, respectively. The yellow and cyan regions indicate charge accumulation and depletion, respectively. The colour bar represents the variation from charge accumulation (yellow) to charge depletion (cyan).

and indicates a physisorption process. The charge redistribution indicates electron donation from the CO molecule to the surface, confirming n-type behaviour.

3.4. Band structure analysis of $In_2O_3(001)$ and Er-doped $In_2O_3(001)$ surfaces

The band structure plots of pure and Er-doped In_2O_3 surfaces are shown in Fig. 3. The band structure analysis confirms that both the pure and Er-doped In_2O_3 exhibit a direct band gap.[26] The Er-doping increases the band gap of the In_2O_3 surface compared to the bulk In_2O_3 system.[27] The band gap value increases from 0.11 eV to 0.17 eV. For the Er-doped In_2O_3 surface the band structure in the conduction band is denser than the pure In_2O_3 surface, which reflects the presence of defect surfaces after doping. Also, the Fermi energy level slightly shifts towards the conduction band. The changes in band structure reflect the change in electronic properties of the material. Also, the calculated band gaps for pure and doped In_2O_3 surfaces are very small, indicating near-metallic behaviour. Despite this, the adsorption of gas molecules (H_2S, NO_2, and CO) can still modulate surface electronic properties through charge transfer, producing a measurable sensing response. Er doping slightly increases the band gap by introducing localized states near the Fermi level, which enhances charge transfer interactions and improves gas-sensing performance. It should also be noted that DFT calculations using local or gradient-corrected exchange–correlation potentials are known to severely underestimate the band gap of semiconducting materials.[15] Therefore, while the absolute band gap values appear smaller, the relative trends and electronic structure changes remain physically meaningful, supporting the proposed sensing mechanism governed primarily by surface charge redistribution rather than large band gap modulation (discussed in Section 4).

3.5. Density of states (TDOS and PDOS) analysis

For further confirmation, DOS and PDOS analyses have been conducted. The density of states (DOS) and partial density of states (PDOS) have been evaluated for the surface before adsorption of gas molecules and after adsorption of gas molecules.

The total density of states and partial density of states for the pure $In_2O_3(001)$ surface are shown in Fig. 4(a). It indicates that in TDOS the main contribution is due to the oxygen atoms, while a minor contribution is observed from the indium (In) atoms. Valence band states have concentrated DOS peaks while the conduction band region exhibits low intensity of DOS peaks. Also, band gaps are observed in between the highest occupied state and lower unoccupied state indicating its semiconducting behaviour. For Er-doped In_2O_3, the DOS contribution of Er is mainly from the p and d orbitals (as shown in Fig. 4(b)). The contribution of Er is observed only in the conduction band, indicating the creation of new states or defect surfaces. These defects are useful for gas sensing applications.

After H_2S adsorption on the $In_2O_3(001)$ surface, the DOS peak intensity decreases from the $In_2O_3(001)$ surface, indicating an interaction between the surface and H_2S gas molecule (as shown in Fig. 4(c)). The partial DOS (PDOS) of indium (In) atoms enhances after H_2S adsorption, suggesting a strong interaction between the $In_2O_3(001)$ surface and H_2S molecule. Oxygen atoms contribute significantly to the total DOS (TDOS), similar to the $In_2O_3(001)$ surface. The PDOS contributions from hydrogen (H) and sulphur (S) atoms are also observed in Fig. 4(d). However, after Er doping into the $In_2O_3(001)$ surface, the PDOS contributions from hydrogen (H) and sulphur (S) atoms decrease, indicating that the interaction between H_2S and the surface is weakened due to Er incorporation (as shown in Fig. 4(d)). Additionally, the TDOS and PDOS of oxygen atoms increase, and the Er contribution appears mainly in the conduction band region. This suggests that Er doping reduces the strength of H_2S on the In_2O_3 surface.

Also, in NO_2 adsorption, the valence band is dominated by oxygen (O) PDOS with O 2p states. The nitrogen (N) contribution is seen at energies just above 2 eV, which indicates that NO_2 introduces molecular orbitals in the conduction band region, without strongly disturbing the valence band (as shown in Fig. 4(e)). Any significant DOS peaks are not observed exactly at the Fermi level, indicating low charge transfer from pure In_2O_3 to NO_2. This suggests physisorption or weak chemisorption of NO_2 on the surface. For the Er–$In_2O_3(001)$ surface after adsorption of NO_2 a large DOS peak is observed right at the Fermi level, mainly contributed by Er and N (as shown in Fig. 4(f)).[28] The alteration of TDOS and PDOS peaks after adsorption of a NO_2 molecule indicates that the electronic structure changes. The overall electronic structure is altered, and the interaction is stronger than that of pure In_2O_3, indicating strong adsorption of gas molecules.

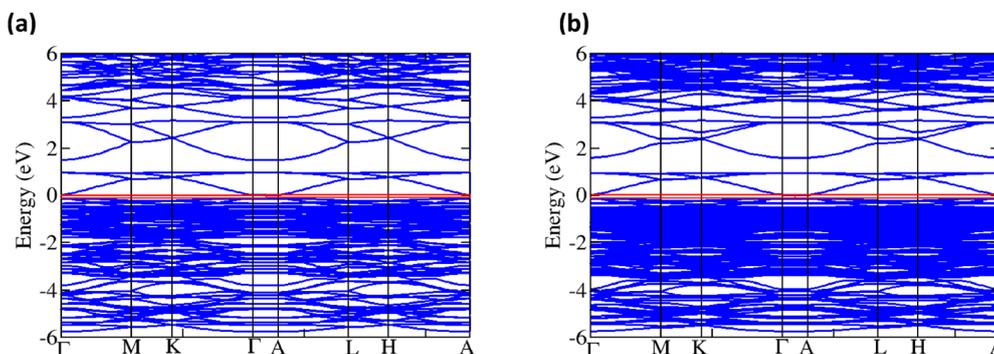After adsorption of CO gas molecules on the In_2O_3 and Er-doped In_2O_3 surface the changes in TDOS and PDOS are

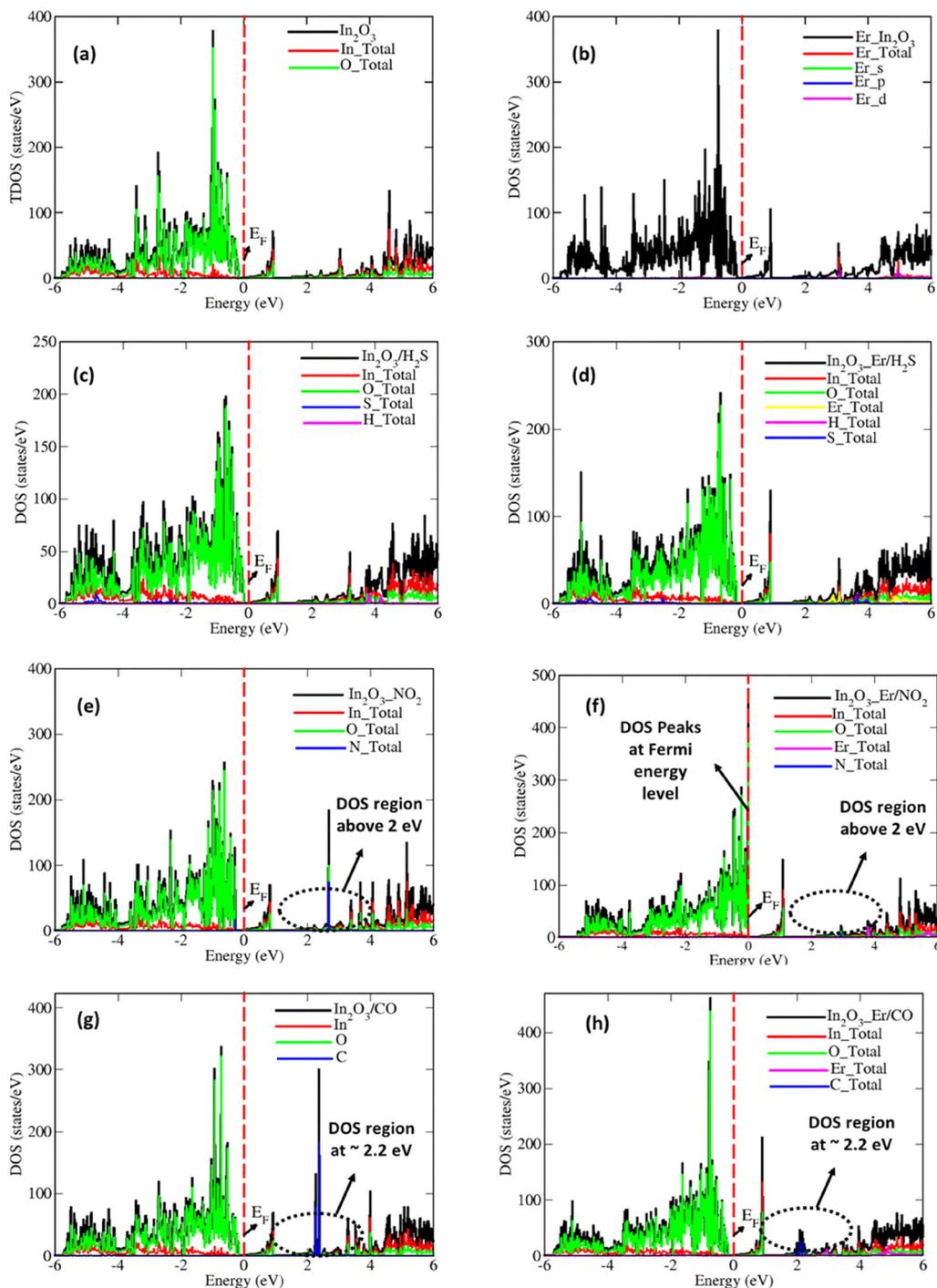**Fig. 3** Band structure for the (a) pure $In_2O_3(001)$ surface and (b) Er-doped $In_2O_3(001)$ surface.

Fig. 4 Total and partial density of states (DOS and PDOS) of (a), (c), (e) and (g) pure and (b), (d), (f) and (h) Er-doped In$_2$O$_3$(001) surfaces: (a) and (b) without gas adsorption, (c) and (d) after H$_2$S adsorption, (e) and (f) after NO$_2$ adsorption, and (g) and (h) after CO adsorption. The red dotted line indicates the Fermi energy level.

slightly modified. The carbon (C) related sharp peak at ~2.2 eV represents the CO molecular orbital contribution (as shown in Fig. 4(g)). This state lies well above the Fermi level, suggesting weak electronic interaction and minimal charge transfer between CO and the In$_2$O$_3$ surface. There being no new states near the Fermi level indicates physisorption or weak chemisorption of CO on pure In$_2$O$_3$. The band gap is preserved,

with no significant mid-gap state formation. For the Er-doped In$_2$O$_3$ surface the C-related peak at ~2.2 eV becomes slightly broader and less intense, and new states appear closer to the Fermi level, indicating a stronger interaction than in the undoped system (as shown in Fig. 4(h)). Some Er-related states overlap with the O and C contributions, especially just below and above the Fermi level. This suggests hybridization and possible weak charge
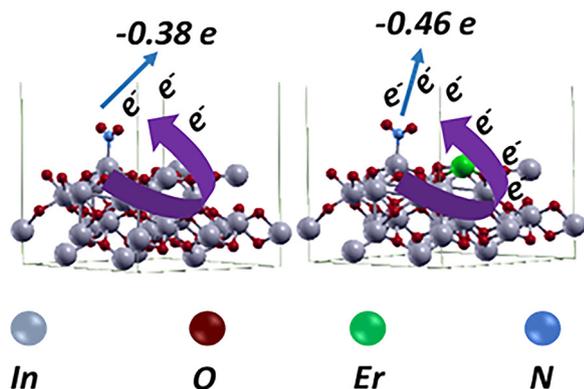
This journal is © the Owner Societies 2025

Phys. Chem. Chem. Phys., 2025, **27**, 25440–25448 | **25445**

Fig. 5 NO$_2$ gas sensing mechanism diagram on both the pure and Er-doped In$_2$O$_3$ surfaces.

exhibits a negative charge transfer of -0.38 e, indicating electron withdrawal from the n-type metal oxide. Upon erbium (Er) doping, the charge transfer becomes more negative (-0.46 e), evidencing stronger electron extraction by NO$_2$. This enhanced electron withdrawal widens the surface depletion layer and increases the sensor resistance in comparison to the Er-doped surface. Consistent with this, the electronic-structure picture is that NO$_2$ introduces acceptor-like states near the Fermi level more strongly in Er-doped In$_2$O$_3$, promoting chemisorption and greater carrier depletion (as shown in Fig. 5). Therefore, erbium (Er) doping tunes the surface electronic environment to favour NO$_2$ adsorption and response, predicting higher selectivity to NO$_2$ compared with the undoped material.

transfer. However, the change is not as significant as observed with NO$_2$ adsorption, indicating that Er doping enhances the CO interaction only slightly, likely weak chemisorption.

4. Gas sensing mechanism

Bader charge analysis was used to elucidate the adsorption mechanism of NO$_2$ on In$_2$O$_3$. On the pure In$_2$O$_3$ surface, NO$_2$

5. Future scope

In the present study, the electronic structure and gas adsorption behaviour of Er-doped In$_2$O$_3$ surfaces were thoroughly investigated for H$_2$S, NO$_2$ and CO gases. To expand on this research, future studies could explore the adsorption characteristics of Eu-doped In$_2$O$_3$ surfaces. Preliminary DFT calculations (Bader charges and DOS calculations as shown below) on Eu-doped In$_2$O$_3$ without gas adsorption have already been performed, revealing notable changes in the electronic structure compared to Er doping.

Table 2 Bader charge of the respective In, Er_1, Eu_1 and O atoms for In$_2$O$_3$(001), Er-doped In$_2$O$_3$(001), and Eu-doped In$_2$O$_3$(001) systems

Atoms		Bader charge		Bader charge		Bader charge	
In, O, Er_1 and Eu_1		Pure In$_2$O$_3$(001) surface (In1 to In12)	Pure In$_2$O$_3$(001) surface (In13 to In24)	Er-doped In$_2$O$_3$(001) surface (In1 (replaced (In1 from Er_1) to In12)	Er-doped In$_2$O$_3$(001) surface (In13 to In24)	Eu-doped In$_2$O$_3$(001) surface (In1 (replaced (In1 from Eu_1) to In12)	Eu-doped In$_2$O$_3$(001) surface (In13 to In24)
In1	In13	1.725	1.725	Er_1(2.06)	1.710	Eu_1(2.04)	1.709
O1	O17	-1.185	-1.185	-1.191	-1.275	-1.192	-1.261
O2	O18	-1.186	-1.186	-1.277	-1.191	-1.262	-1.191
O3	O19	-1.187	-1.187	-1.192	-1.195	-1.191	-1.195
In2	In14	1.855	1.854	1.861	1.861	1.862	1.860
In3	In15	1.869	1.869	1.874	1.873	1.871	1.872
O4	O20	-1.245	-1.245	-1.248	-1.245	-1.242	-1.245
O5	O21	-1.246	-1.246	-1.245	-1.250	-1.244	-1.250
O6	O22	-1.245	-1.245	-1.245	-1.243	-1.244	-1.242
In4	In16	1.867	1.867	1.887	1.866	1.888	1.865
In5	In17	1.856	1.856	1.856	1.856	1.856	1.856
O7	O23	-1.138	-1.138	-1.137	-1.138	-1.137	-1.138
O8	O24	-1.139	-1.139	-1.138	-1.139	-1.138	-1.139
O9	O25	-1.137	-1.137	-1.136	-1.137	-1.136	-1.137
In6	In18	1.537	1.537	1.533	1.533	1.533	1.533
In7	In19	1.725	1.725	1.707	1.708	1.705	1.708
O10	O26	-1.185	-1.185	-1.191	-1.188	-1.192	-1.189
O11	O27	-1.186	-1.186	-1.193	-1.188	-1.193	-1.189
O12	O28	-1.188	-1.187	-1.277	-1.918	-1.264	-1.192
In8	In20	1.854	1.854	1.854	1.863	1.852	1.861
In9	In21	1.869	1.869	1.872	1.867	1.871	1.865
O13	O29	-1.245	-1.245	-1.248	-1.244	-1.248	-1.244
O14	O30	-1.246	-1.246	-1.245	-1.248	-1.245	-1.248
O15	O31	-1.245	-1.245	-1.248	-1.245	-1.248	-1.245
In10	In22	1.867	1.867	1.866	1.866	1.866	1.865
In11	In23	1.856	1.856	1.856	1.856	1.856	1.857
O16	O32	-1.138	-1.138	-1.138	-1.138	-1.138	-1.139
O17	O33	-1.139	-1.139	-1.139	-1.139	-1.140	-1.139
O18	O34	-1.137	-1.137	-1.137	-1.137	-1.138	-1.137
In12	In24	1.537	1.537	1.533	1.534	1.533	1.533

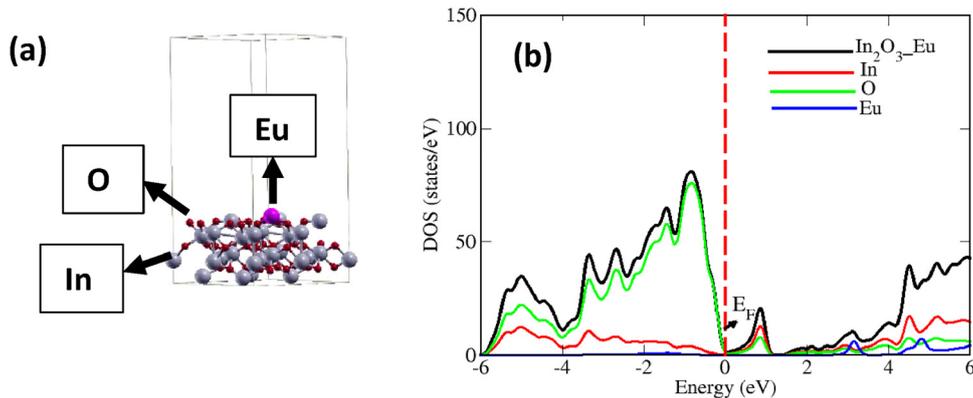Er_1 and Eu_1 are the dopants replaced by first indium (In) atom.

Fig. 6 (a) Optimized geometry of Eu-doped In_2O_3 obtained from DFT calculations. (b) Corresponding total and partial density of states (TDOS and PDOS) of the Eu-doped $In_2O_3(001)$ surface.

Bader charge analysis was conducted to evaluate the effect of Er and Eu doping on the $In_2O_3(001)$ surface. In the doped systems, the Er and Eu atoms exhibit Bader charges of 2.06 e and 2.04 e, respectively (as shown in Table 2), indicating partial electron donation to the surrounding lattice. This electron redistribution alters the local electronic environment, which can influence gas adsorption behaviour. Notably, nearby oxygen atoms (O1, O2) show charges of -1.275 and $-1.277e$, respectively, which are more negative than the pure system (-1.185 and $-1.186e$). For Eu-doping, O1 and O2 also become more negative (-1.261 and $-1.262e$). These results indicate localized electron accumulation around the oxygen atoms, possibly due to the higher electronegativity and ionic character of the dopants compared to indium (In) atoms. The indium (In) atoms remain largely unaffected across all systems, indicating structural stability.

The optimized structure of Eu-doped In_2O_3 is shown in Fig. 6(a). The TDOS and PDOS of Eu-doped In_2O_3 are shown in Fig. 6(b). The contribution in the DOS structure near the Fermi level indicates the presence of defect states introduced by Eu doping. The peak around ~ 0.85 eV likely corresponds to the hybridization between O 2p states and indium (In) atoms (as shown in Fig. 6(b)). The observed band gap is useful for the enhancement in the electrical conductivity, which is crucial in sensing applications.

6. Limitation

While DFT calculations provide results at 0 K and consider only static adsorption energies, these results provide crucial atomistic-level insight into gas–surface interactions that cannot be directly accessed experimentally. In real sensor operation, factors such as temperature, adsorption/desorption kinetics, and desorption energy barriers influencing sensitivity, selectivity, and recovery are also involved. Nevertheless, the calculated adsorption energies, Bader charge transfer, and electronic structure reveal how Er-doping modulates surface reactivity and enhances NO_2 adsorption. These predictive insights serve as a reliable guideline for experimental optimisation, helping to identify promising dopants, surface sites, and gas-specific interactions prior to costly sensor fabrication. Therefore, even without explicitly including kinetic/thermal effects, the present study offers valuable mechanistic understanding that complements and guides future investigations.

7. Conclusion

The effect of rare earth element (Er) doping in In_2O_3 for gas sensing applications was investigated. DFT calculations were performed to analyse the sensing behaviour of H_2S, NO_2 and CO gas on both pristine and Er-doped $In_2O_3(001)$ surfaces. The gas sensing behaviour was evaluated through adsorption energy, Bader charge analysis, charge transfer, TDOS and PDOS analysis. The main conclusions are as follows:

(I) Er-doping significantly alters the adsorption energy for gas molecules. For H_2S, the adsorption energy is stronger or more favourable for the pristine surface (-0.53 eV) while for the Er-doped surface it is less negative (-0.42 eV), indicating reduced interaction. For the CO molecule, a slight decrease is observed (from -0.25 to -0.19 eV). In contrast, the adsorption energy for the NO_2 molecule enhances from -0.37 to -0.61 eV upon Er doping, indicating enhanced interaction and suggesting that the Er-doped $In_2O_3(001)$ surface is more favourable for selective NO_2 gas detection.

(II) Bader charge analysis supports these observations. For H_2S gas, charge transfer decreases from $+0.40$ e (pristine) to $+0.09$ e (Er-doped surface) and for CO the changes are minor. However, for NO_2, charge transfer increases from -0.38 e (pristine) to -0.46 e (Er-doped), confirming stronger interaction upon doping.

(III) Band structure results indicate changes in the electronic structure after Er doping, reflecting the impact of dopant states.

(IV) TDOS and PDOS analyses reveal that after NO_2 adsorption on the Er-doped In_2O_3 surface, new states appear near the Fermi energy, indicating strong electronic interaction.

Conflicts of interest

The authors declare that they have no known financial or non-financial conflicts of interest that could have appeared to influence the work reported in this paper.

Data availability

The datasets generated and analyzed during the current study, including input and output files from Quantum Espresso calculations, are available from the corresponding author on reasonable request.

Acknowledgements

References

1 S. Bilge, *et al.*, Recent advances in flower-like nanomaterials: Synthesis, characterization, and advantages in gas sensing applications, *TrAC, Trends Anal. Chem.*, 2022, **153**, 116638.

2 D. Kohl, Function and applications of gas sensors, *J. Phys. D: Appl. Phys.*, 2001, **34**(19), R125.

3 Y. Liu, *et al.*, Pristine and Ag decorated In_2O_3 (110): A gas-sensitive material to selective detect NO2 based on DFT study, *J. Mater. Res. Technol.*, 2022, **18**, 4236–4247.

4 Y. Yoon, *et al.*, Metal-oxide nanomaterials synthesis and applications in flexible and wearable sensors, *ACS Nanosci. Au*, 2021, **2**(2), 64–92.

5 T. Suzuki, *et al.*, Significant increase in band gap and emission efficiency of In_2O_3 quantum dots by size-tuning around 1 nm in supermicroporous silicas, *Langmuir*, 2017, **33**(12), 3014–3017.

6 L. Guo, *et al.*, Preparation and gas-sensing performance of In_2O_3 porous nanoplatelets, *Sens. Actuators, B*, 2011, **155**(2), 752–758.

7 Y. Bai, *et al.*, Conductometric isopropanol gas sensor: Ce-doped In_2O_3 nanosheet-assembled hierarchical microstructure, *Sens. Actuators, B*, 2023, **377**, 133007.

8 H. Wu, *et al.*, Ni-decorated WS_2-WSe_2 heterostructure as a novel sensing candidate upon C_2H_2 and C_2H_4 in oil-filled transformers: a first-principles investigation, *Mol. Phys.*, 2025, e2492391.

9 W. Yang, T. Chen and G. Zhou, Unveiling the tunable electronic, optoelectronic, and strain-sensitive gas sensing properties of Janus ZrBrCl: Insights from DFT study, *Appl. Surf. Sci.*, 2025, **680**, 161283.

10 N. Sharma and S. P. Choudhury, Gas sensing using metal oxide semiconductor doped with rare earth elements: A review, *Mater. Sci. Eng., B*, 2024, **307**, 117505.

11 J. Zhou, *et al.*, Rare earth element Ce-doped floral In_2O_3 with high sensing performance for n-butanol, *Vacuum*, 2025, **231**, 113761.

12 X. Wang, *et al.*, High response gas sensors for formaldehyde based on Er-doped In_2O_3 nanotubes, *J. Mater. Sci. Technol.*, 2015, **31**(12), 1175–1180.

13 Z. Qin, *et al.*, Highly sensitive alcohol sensor based on a single Er-doped In_2O_3 nanoribbon, *Chem. Phys. Lett.*, 2016, **646**, 12–17.

14 W. Chen, *et al.*, A single Eu-doped In_2O_3 nanobelt device for selective H_2S detection, *Sensors*, 2015, **15**(12), 29950–29957.

15 L. S. Pedroza, A. J. da Silva and K. Capelle, Gradient-dependent density functionals of the Perdew-Burke-Ernzerhof type for atoms, molecules, and solids, *Phys. Rev. B:Condens. Matter Mater. Phys.*, 2009, **79**(20), 201106.

16 M. Voccia, *et al.*, Atomic and electronic structures of Co-doped In_2O_3 from experiment and theory, *ACS Appl. Mater. Interfaces*, 2024, **16**(23), 30157–30165.

17 N. Sharma, *et al.*, Gas-Sensing Properties of NO on Ce-Doped Zinc Oxide: A DFT Study, *Part. Part. Syst. Charact.*, 2025, **42**(1), 2400126.

18 R. Deji, *et al.*, Adsorption chemistry of co-doped graphene nanoribbon and its derivatives towards carbon based gases for gas sensing applications: quantum DFT investigation, *Mater. Sci. Semicond. Process.*, 2022, **146**, 106670.

19 Y. Qian and H. Yang, Computational insight into the bioapplication of 2D materials: A review, *Nano Today*, 2023, **53**, 102007.

20 M. J. Spencer and I. Yarovsky, ZnO nanostructures for gas sensing: Interaction of NO_2, NO, O, and N with the ZnO (1010) surface, *J. Phys. Chem. C*, 2010, **114**(24), 10881–10893.

21 N. Sharma and S. P. Choudhury, First-principles study of metal oxide semiconductors for gas sensing applications: A brief review, *Mod. Phys. Lett. B*, 2023, 2342012.

22 A. Abbasi, Tuning the structural and electronic properties and chemical activities of stanene monolayers by embedding 4d Pd: a DFT study, *RSC Adv.*, 2019, **9**(28), 16069–16082.

23 S. Gulshanah and A. Bhattacharjee, Adsorption of η2 (O, C)-tilted formaldehyde geometry on transition metal substituted p (2× 1) SnO_2 (1 1 0) surface: A first-principles analysis, *Chem. Phys.*, 2025, **589**, 112511.

24 S. Shah, *et al.*, NO_2 gas sensing responses of In_2O_3 nanoparticles decorated on GO nanosheets, *Ceram. Int.*, 2022, **48**(9), 12291–12298.

25 A. M. Mebed, *et al.*, Adsorption of CO over the Heusler alloy CrCoIrGa (001) surface: first-principles insights, *RSC Adv.*, 2022, **12**(28), 17853–17863.

26 A. S. de Brito, *et al.*, Structural, optical, and magnetic characterization of Er-doped In_2O_3 nanoparticles, *J. Alloys Compd.*, 2024, **990**, 174353.

27 A. Ghosh, *et al.*, GLAD synthesised erbium doped In_2O_3 nano-columns for UV detection, *J. Mater. Sci.: Mater. Electron.*, 2019, **30**(13), 12739–12752.

28 S. Zhao, J. Xue and W. Kang, Gas adsorption on MoS_2 monolayer from first-principles calculations, *Chem. Phys. Lett.*, 2014, **595**, 35–42.

25448 | *Phys. Chem. Chem. Phys.*, 2025, **27**, 25440–25448

This journal is © the Owner Societies 2025